Physiological Measurement

ACCEPTED MANUSCRIPT • OPEN ACCESS

Simultaneous EIT and EEG using frequency division multiplexing

To cite this article before publication: James Avery *et al* 2019 *Physiol. Meas.* in press https://doi.org/10.1088/1361-6579/ab0bbc

Manuscript version: Accepted Manuscript

Accepted Manuscript is "the version of the article accepted for publication including all changes made as a result of the peer review process, and which may also include the addition to the article by IOP Publishing of a header, an article ID, a cover sheet and/or an 'Accepted Manuscript' watermark, but excluding any other editing, typesetting or other changes made by IOP Publishing and/or its licensors"

This Accepted Manuscript is **© 2018 Institute of Physics and Engineering in Medicine**.

As the Version of Record of this article is going to be / has been published on a gold open access basis under a CC BY 3.0 licence, this Accepted Manuscript is available for reuse under a CC BY 3.0 licence immediately.

Everyone is permitted to use all or part of the original content in this article, provided that they adhere to all the terms of the licence https://creativecommons.org/licences/by/3.0

Although reasonable endeavours have been taken to obtain all necessary permissions from third parties to include their copyrighted content within this article, their full citation and copyright line may not be present in this Accepted Manuscript version. Before using any content from this article, please refer to the Version of Record on IOPscience once published for full citation and copyright details, as permissions may be required. All third party content is fully copyright protected and is not published on a gold open access basis under a CC BY licence, unless that is specifically stated in the figure caption in the Version of Record.

View the article online for updates and enhancements.

This content was downloaded from IP address 128.41.35.179 on 06/03/2019 at 17:58

Simultaneous EIT and EEG using Frequency Division Multiplexing

James Avery[1*], Tom Dowrick[2,3*], Anna Witkowska-Wrobel[3], Mayo Faulkner[3], Kirill Aristovich[3], David Holder[3]

[1] Department of Surgery and Cancer, Imperial College London, London, W2 1PF, UK

E-mail: `james.avery@imperial.ac.uk`

[2]Wellcome/EPSRC Centre for Surgical and interventional Sciences, London W1W 7TS, UK

[3]Department of Medical Physics and Biomedical Engineering,University College London, London WC1E 6BT, UK

[*] These authors contributed equally to this work

Abstract. Objective: Methods have previously been reported for simultaneous EIT and EEG recording, but these have relied on post-hoc signal processing to remove switching artefacts from the EEG signal and require dedicated hardware filters and the use of separate EEG and EIT electrodes. This work aims to demonstrate that an uncorrupted EEG signal can be collected simultaneously with EIT data by using frequency division multiplexing (FDM), and to show that the EIT data provides useful information when compared to EEG source localisation.

Approach: A custom FDM EIT current source was created and evaluated in resistor phantom and neonatal head tank experiments, where a static and dynamic perturbation was imaged. EEG and EIT source localisation were compared when an EEG dipole was placed in the tank. EEG and EIT data were collected simultaneously in a human volunteer, using both a standard EEG and a Visual Evoked Potential (VEP) paradigms.

Main Results: Differences in EEG and VEP collected with and without simultaneous EIT stimulation showed no significant differences in amplitude, latency or PSD (p-values > 0.3 in all cases). Compared with EEG source localisation, EIT reconstructions were more accurately able to reconstruct both the centre of mass and volume of a perturbation.

Significance: The reported method is suitable for collecting EIT in a clinical setting, without disrupting the clinical EEG or requiring additional measurement electrodes, which lowers the barrier to entry for data collection. EIT collection can be integrated with existing clinical workflows in EEG/ECoG, with minimal disruption to the patient or clinical team.

Keywords: Electrical Impedance Tomography (EIT), Frequency Division Multiplexing, Electroencephalogram (EEG), Brain imaging, Epilepsy

Submitted to: *Physiol. Meas.*

Accepted Manuscript

1. Introduction

Epilepsy is one of the most common neurological conditions worldwide, with approximately 50 million people affected Meinardi et al. (2008). Of these patients, some will be resistant to anti-epileptic drugs, and may require surgical intervention to remove the affected areas of the brain. Being able to accurately localise and potentially image the seizure onset area is a critical presurgical step. Intracranial electroencephalography (EEG) methods are the most commonly used for localisation (Benbadis et al., 2004), which has the highest spatiotemporal resolution among current clinical methods for seizure monitoring. The main intracranial EEG monitoring methods are subdural grids, strips (electrocorticography, ECoG), and depth electrodes (stereo-EEG, SEEG). While these techniques have been successfully used for patient benefit, there are some associated limitations. Epileptic discharges may not have ECoG correlates if they originate >5 mm away from the contact boundary (von Ellenrieder et al., 2012) i.e in deeper subcortical structures; or if the source is oriented tangentially to electrodes (Burle et al., 2015; Ebersole, 1997). Depth electrodes can overcome these issues, but are limited in their spatial sampling volume and, due to the increased invasiveness, may cause functional deficits due to structural brain damage (Wellmer et al., 2012).

Additional limitations of ECoG and depth electrode techniques are that they are prohibitively invasive for cases of neonatal epilepsy, and they are not suitable for cases of electroclincial dissociation, where clinical symptoms of seizure are present but not in EEG recordings (Weiner et al., 1991; Murray et al., 2008). There exists, therefore, a clinical need for improved presurgical evaluation to enable more precise localisation of the epilepsy onset zone.

Electrical Impedance Tomography (EIT) is a technique where an image of the internal structure of an object can be reconstructed from surface impedance measurements (Holder, 2004), with the most successful applications of EIT reported in imaging organs of the torso (lungs, liver, breast). EIT has also been used to image fast neural activity in the brain (Aristovich et al., 2016) including epilepsy (Hannan, Faulkner, Aristovich, Avery, Walker and Holder, 2018).

There are two distinct impedance changes during epileptic activity to which EIT is sensitive. The first, referred to as the fast change (lasting several ms), is caused by depolarisation of local neuronal populations due to the opening of voltage-dependent ion channels during epileptic activity (Vongerichten et al., 2016). The second impedance signal, the slow change, is longer-lasting, due to changes in cerebral tissue impedance over several seconds during seizures (Harreveld and Schadé, 1962; Vongerichten et al., 2016; Wang et al., 2017; Hannan, Faulkner, Aristovich, Avery, Walker and Holder, 2018). This is caused by cell swelling, and the associated impedance change can either precede or follow the electrographic changes associated with the epileptic events (Andrew and Macvicar, 1994; Broberg et al., 2008; Binder and Haut, 2013)

EIT has previously been proposed as an adjunct to conventional invasive or non-invasive EEG monitoring methods, for improving the preoperative localisation of seizure

Accepted Manuscript

foci (Boone et al., 1994; Fabrizi et al., 2006), and the feasibility of EIT using depth electrodes has been demonstrated (Witkowska-Wrobel et al., 2018). The EIT and EEG inverse problems are similar, but EIT offers advantages with a greater number of independent measurements for the same number of electrodes, a theoretically unique solution and is not sensitive to dipole orientation (Aristovich et al., 2018; Somersalo et al., 1992) However, due to limitations with existing EIT systems, it has not yet been possible to validate the collection of EIT data alongside EEG for clinical recordings, severely limiting its clinical potential.

1.1. EIT Hardware

It is possible to obtain EIT measurements using an EEG amplifier, with only the addition of a current source to inject current between pairs of electrodes in sequence. However, to minimise interruption of clinical procedures, several requirements can be placed on an EIT system for it to be deployed for simultaneous EEG/ECoG recordings:

(i) In order to correlate impedance changes to epileptic activity, EIT data should be recorded simultaneously with EEG data, using the same electrodes.
(ii) The EIT equipment should not affect the EEG signal

When measurements are made as part of an existing clinical workflow used for diagnosis or treatment, care must be taken to avoid any disruption to the relevant medical data, which may introduce additional requirements on a case-by-case basis.

Requirement 2 precludes the use of any EIT system which employs switching of recording or injection electrodes, as this introduces artefacts into the EEG signal. While post-hoc correction of EEG artefacts has been demonstrated (Fabrizi et al., 2010), this requires dedicated hardware filters and the use of separate EIT and EEG electrodes, contradicting Requirement 1. Crucially, sequential measurement and injection is not suitable for detecting infrequent spontaneous epileptic events, where a full imaging protocol cannot be obtained through coherent averaging.

Both requirements mean that injecting current between sequential pairs of electrodes, known as Time Division Multiplexing (TDM) is not suitable. However, these requirements can be satisfied using Frequency Division Multiplexing (FDM) EIT. In FDM-EIT current is injected at multiple frequencies simultaneously through different electrode pairs, and thus continuously collects a full EIT protocol and removes the need to switch injection pairs. The disadvantages of this technique are the greater complexity of the current source hardware, signal processing and reduced EIT protocols (Dowrick and Holder, 2018).

1.2. Experimental Design

In this work we investigate the extent to which clinically relevant EEG can be obtained simultaneous to FDM-EIT data. First the noise performance of an updated six channel FDM-EIT system by Dowrick and Holder (2018) is measured in resistor phantom

Accepted Manuscript

experiments. Then experiments in a human volunteer characterise the effect of the addition of EIT signals upon the frequency and transient response of clinically important EEG measures. As it was not possible to measure epileptic changes in these experiments, an ECG gated cardiosynchronous signal with similar time course and conductivity changes (Braun et al., 2018) is used to demonstrate the sensitivity of the EIT system. Finally, to demonstrate whether potentially diagnostically relevant information can still be obtained from EIT reconstructions when using a reduced protocol, images were made using an improved neonatal head tank (Avery, Aristovich, Low and Holder, 2017) and the accuracy compared to EEG inverse source modelling.

2. Methods

2.1. EIT Hardware

The EIT system used for data collection was a refined version of that reported in Dowrick and Holder (2018), comprising a custom 6-channel current source Printed Circuit Board (PCB) and the actiCHamp EEG system (Brain Products GmbH). Full details of the system are given in Appendix B. The EIT current injection protocol was selected using a modification of the algorithm by Faulkner et al. (2017) to select only unique injection pairs. The brain cavity was divided into five regions, and the injection protocol found which maximises the total current density with an approximate even distribution between all regions (within 10%). For the tank this was performed on same mesh used for reconstructions, and on an example generic head mesh used in a stroke study (Goren et al., 2018). The current amplitude was based on limitations for clinical studies using depth electrodes (Witkowska-Wrobel et al., 2018) with an amplitude of 60 μA for all injection pairs, and frequencies above 1.5 kHz, to ensure the SEEG signal is not contaminated. The frequencies used were 1.5 kHz, 2 kHz, 2.5 kHz, 3.5 kHz, 5 kHz and 5.5 kHz, for six injections on the scalp. The inconsistent spacing was chosen to avoid noise introduced by the actiCHamp EEG system, which has a peak at 4 kHz. Two PCBs were used simultaneously in the tank experiments for a total of 12 injections, with 6 kHz, 6.5 kHz, 7 kHz, 7.5 kHz and 8 kHz added. A 20th order Butterworth filter with a bandwidth of 100 Hz was applied around each carrier frequency, after which the amplitude of the signal was extracted using the Hilbert transform. All noise measurements are presented as mean $\pm$ standard deviation in absolute values, and as a ratio of the mean to standard deviation both as Signal-To-Noise (SNR) in dB and as a percentage.

2.2. Resistor Phantom Measurements

Noise, SNR, Total Harmonic Distortion (THD) and inter-channel variation measurements (i.e. comparing the current magnitude across all 6 current sources) were measured on a 32-electrode resistor phantom, comprising 96 resistors, with values between 330 Ω and 1k Ω and the resistance between two adjacent electrodes was 2.7 kΩ. Values

Accepted Manuscript

were calculated using 1 second of data, taken from the middle of a 10 second recording.

2.3. Scalp Recordings

2.3.1. EEG EEG and EIT measurements were made in a single human volunteer, with 21 scalp Ag/AgCl EEG cup electrodes (10mm radius, Micromed Electronics Ltd, England) in accordance with the the International 10-20 Electrode Positioning System (Oostenveld and Praamstra, 2001) with additional ground and reference electrodes placed along the midline at CPz and FCz respectively, a standard VEP montage (Walsh, 2005). Experiments were approved by the UCL Research Ethics Committee. The subject's skin was prepared before placing the electrodes to minimise the electrode-skin impedance, remove dirt, grease and the external *stratum corneum* layer of skin cells from the surface (Rosell et al., 1988). The skin at each contact site was rubbed with ethanol and then with abrasive gel (NuPrep, Weaver and Company, USA) applied using cotton buds before applying conductive EEG paste (Ten20 Conductive, Neurodiagnostic Electrode Paste, Weaver and Company, USA). Finally, the electrodes were then secured with tape. ECG was also recorded using a non clinical montage using two electrodes placed in the second intercostal space on the midclavicular line, using the same reference and ground EEG electrodes. This was filtered using a 1 Hz 2nd order Butterworth high pass filter, a 4th order 100 Hz Butterworth low pass filter and a 50 Hz 2nd order notch filter with Q factor 35.

Spontaneous EEG was recorded during an awake state, with 30 second periods of eyes open and closed, for a total of 10 minutes. This was performed first with no EIT system connected and repeated with the EIT system connected and active. The EEG signals were filtered using a 2nd high pass and 6th order low pass Butterworth filters with 1 Hz and 400 Hz cut off frequencies respectively. The power spectral density (PSD) for each 30 period was estimated using the Thompson Multitaper estimate method, with a time-halfbandwidth product of 10, for 1 Hz bins between 0-50 Hz. To identify the effect of the addition of the EIT current injection, a two-tailed paired t-test was performed on the spectral density in each 1 Hz frequency bin ($P < 0.01$) for both the open and closed case.

2.3.2. Visual Evoked Potentials VEPs are a common clinical test, where EEG data is recorded from the visual cortex, in response to either a flash stimulation or pattern reversal stimulation (NeurophysiologySociety, 2006). Clinically, this can provide information about abnormal conduction in the visual pathway and therefore it is widely used for assessment of conditions such as demyelination, optic neuritis or other neuropathies (Walsh, 2005).

A VEP pattern-reversal stimulation paradigm was used (NeurophysiologySociety, 2006). Visual responses were evoked with $0.6\,^{\circ}$ black and white chequerboard presented 75 cm in front of the subject on a laptop screen, reversing at 2 Hz for 180 sec and repeated twice. The stimulation was controlled by MATLAB code, using the PyschToolbox

Accepted Manuscript

(`http://psychtoolbox.org/`) to adjust the cheque size, focusing point (cross) and the stimulation latency. A photodiode placed at the corner of the screen was recorded through an auxiliary channel on the actiCHamp, to capture the reversal triggers and enable synchronisation of the recorded data. The subject sat in a darkened room, with eyes opened and focused on the cross in the middle of the screen during VEP stimulation. Only voltages recorded in the three electrodes spanning the occipital region - O1, OZ and O2, were considered in subsequent analysis. In this case only electrode O1 was used for current injection, with the others as measurement only. The VEP data was filtered according to the American Clinical Neurophysiology Society Guidelines (NeurophysiologySociety, 2006), using a 2nd order 200 Hz low pass Butterworth filter and a first order 1 Hz high pass filter. Whilst guidelines state that it is preferential to avoid the use of a notch filter, a 6th order 50 Hz notch filter with 1 Hz bandwidth was found to be necessary in these experiments on electrodes where EIT current was also being injected. The final traces were then obtained using coherent averaging of c. 720 reversals. As with the spontaneous EEG experiments, VEPs were recorded first with only the EEG system connected, and then with the EIT system connected and injecting current.

To investigate the effect of the addition of EIT on the VEP signals, the amplitude and latency of the two most clinically relevant features were extracted. These were the positive component 100 ms after pattern reversal, P100, and the smaller negative component after approximately 145 ms, N145 (Walsh, 2005). First the P100 latency of both for the global average of all 718 repeats for each case was compared. As the VEP signal is only apparent after coherent averaging, two-tailed paired t-test was performed on the P100 peak and latency of averages of 100 repeats, i.e. n=7 for both with and without EIT present.

2.3.3. EIT Cardiosynchronous Signal It was not possible to replicate the exact EIT signals expected during seizures in a healthy volunteer, so a substitute signal was required to demonstrate the capabilities of the system. Previous studies using the visually evoked EIT signals used either a Bipolar square wave current source (Gilad and Holder, 2009), or injected 1 mA at 50 kHz (Tidswell et al., 2001). These signals are similar in amplitude and time course as the fast neural and cell swelling signals respectively. However, these studies used current signals which could not be reproduced in these experiments using FDM-EIT, as they would either introduce switching artefacts, or require frequencies outside the bandwidth of the EEG amplifier used.

EIT waveforms have components that are synchronised with cardiac activity (Halter et al., 2008; Adler et al., 2017), and have been proposed as a non invasive measure of stroke volume of the heart (Braun et al., 2018) and pulmonary artery pressure (Proença et al., 2016). This signal is also present in scalp measurements, whilst commonly not of direct interest in brain applications, the time course of $\approx$ 1s is of the order expected during cell swelling during a seizure (Harreveld and Schadé, 1962; Hannan, Faulkner, Aristovich, Avery, Walker and Holder, 2018) or those observed following an inter ictal

Accepted Manuscript

spike Vongerichten et al. (2016). Commonly carrier frequencies above 50 kHz are used to investigate cardiosynchronous signals (Proença et al., 2016; Braun et al., 2018), but as they are largely resistive structural changes, they are present at the same frequencies as those arising from cell swelling. Further, dependent upon the location on the body where they are measured, cardiosynchronous impedance changes are of the order as those expected on the scalp during seizures, 0.1 % or less Fabrizi et al. (2006).

The ECG gated signal was extracted from the continuous EIT measurements during the spontaneous EEG recordings. The EIT traces were filtered using a 1 Hz 1st order high pass, and 50 Hz 2nd order Butterworth Low pass filters, before coherent averaging of 151 repeats. Due to the non-clinical ECG montage used, S (as opposed to R) was the most prominent component of the QRS complex and was thus used as the trigger for coherent averaging.

2.4. Tank Experiments

A modified version of the 32-channel 130 mm diameter neonatal head tank and perforated skull with realistic conductivity distribution, described by Avery, Aristovich, Low and Holder (2017), was used in all experiments. In this study, the 3D models were altered to incorporate sintered Silver/Silver-Chloride electrodes (Biomed Electrodes, USA) and the alignment of the skull surface perforations to the scalp surface was improved. The tank was filled with 0.2 % saline for a background conductivity of 0.4 S/m in the scalp and brain layers, and the skull conductivity was 0.03 S/m. A laser-cut open source robot arm (MeArm, Mime Industries UK) was mounted on the frame of the tank Figure 1, which allowed for positioning of the perturbation throughout the tank, and complete removal for baseline recordings.

To minimise the displacement of saline during motion of the robot arm, a spherical 3D lattice perturbation 20 mm in diameter and 16% volume fraction was designed using MeshMixer (Autodesk Inc., USA). The perturbation was printed using conductive polylactic acid (cPLA) (Protopasta, USA), which has a rated conductivity of 0.67 S/m, but the effective conductivity of the printed models is dependent upon the layer size and internal structure. The printing parameters and beam thickness were chosen to produce a 10% contrast when placed within a two electrode saline tube phantom, as described in Avery, Aristovich, Low and Holder (2017).

2.4.1. Static Measurements Data were collected with a static perturbation in three locations: anterior, posterior and lateral, Figure 3. In each case, 10 seconds of baseline data were collected before each perturbation was placed inside the tank, with a further 10 seconds of data recorded for each perturbation. The mean amplitude of one second in the middle of the recording was calculated for the baseline and perturbation periods, to produce one set of voltage difference data for each perturbation.

Accepted Manuscript

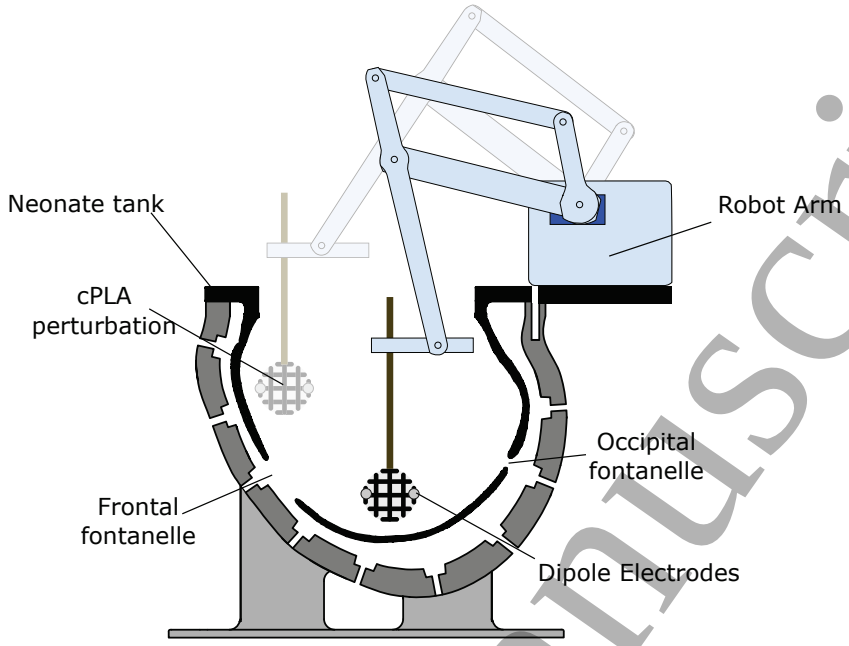

Figure 1. Tank experimental setup. Neonate head phantom with 32 Ag/AgCl electrodes and realistic skull. Current injected simultaneously between 12 pairs of electrodes between 1.5 and 8 kHz. A combined impedance and dipole perturbation positioned by MeArm robot arm mounted on frame of tank.

2.4.2. Comparison to EEG Inverse Source Modelling A dipole representing an EEG source was placed inside the spherical perturbation, to allow a direct comparison between EEG source localisation and EIT. Two 0.32 mm (28 AWG) wires were positioned on the outside of the lattice perturbation, with approximately 0.5 mm of the insulation at the tip exposed. The current dipole was generated using the DAC on an Arduino Due at 50 kHz update frequency and a battery powered, single ended Howland current pump. The input voltage signal was half a second of resting EEG signal recorded in the previous experiment, chosen at random, with a bandwidth of 5 - 300 Hz. The current level was scaled to produce an RMS voltage of 200 μV in the largest channel in the posterior location when oriented parallel to the midline. The effect of the addition of EIT was further investigated by comparing the EEG signals measured on the channel with the largest measured voltage that was also used to inject current. The correlation coefficient was calculated to understand the temporal correlation, PSD and spectral coherence was calculated to investigate any frequency dependent effects. T-tests were performed comparing both the distribution of voltages (1 ms time bins) and power spectral density (1 Hz bins) for all 20 repeats of the EEG signal, with $P < 0.01$. Reconstructions were made at a single time point, at the peak voltage in the EEG sequence.

2.4.3. Dynamic Measurements Often, epileptic activity is not limited to a single location, but can spread from an initial focal onset to secondary or tertiary locations through the recruitment of additional neural circuits Kramer and Cash (2012).

Accepted Manuscript

Therefore, to better represent these impedance changes, dynamic recordings were made where the lattice perturbation was moved between the anterior, posterior and lateral locations in sequence. The speed of the robot arm (Supplementary Materials) was limited to 0.1 m/s to minimise artefactual impedance changes from excessive motion of the saline background. The motion of the motor arm was smoothed further by defining S Curve velocity profiles to minimise sudden changes in acceleration Meckl et al. (1998). One second of baseline data was recorded before commencing robot movement, after which data was recorded continuously. The sequence was repeated twice within a single recording, for a total of 25 seconds. The EIT traces were decimated using a 100 order FIR anti-aliasing filter from a sample rate of 100 kHz to 20 Hz, using four incremental decimation steps, and then low pass filtered using a 20 Hz 2nd order Butterworth filter.

2.5. EIT & EEG Image Reconstruction

A circa 6,000,000 tetrahedral element mesh of the head tank, generated using UCL-MESHER, was used to compute the forward model in PEITS (Jehl et al., 2015) and generate simulated data. EIT images were reconstructed using a circa 200,000 element hexahedral mesh and 0th order Tikhonov algorithm with noise-based correction; the hyper parameter was chosen using leave one out cross validation (Aristovich et al., 2014). The noise based correction assigns each element in the mesh a value according to the significance of the change, rather than an absolute impedance value. Images were rendered using ParaView, with a full-width half-max (FWHM) threshold applied. The EEG inverse problem was implemented using the same methods as Witkowska-Wrobel et al. (2018); Aristovich et al. (2018), which uses the linearised lead-field matrix, calculated using a combination of the adjoint fields theorem and the reciprocity theorem (Vallaghé et al., 2008). Images were reconstructed using the same meshes and 0th order Tikhonov regularisation method.

The quality of the reconstructed images was assessed using three image quantification metrics (Malone et al., 2014):

- Localisation error: the displacement of the centre of mass of the reconstructed perturbation with respect to its real position, as a percentage of the tank's diameter.
- Shape error: the mean of the difference in each axis of the reconstructed perturbation to the perturbation's actual width, expressed as a percentage of the tank's diameter.
- Image noise: the standard deviation of all conductivity changes not belonging to the reconstructed perturbation, expressed as a percentage of the mean of the reconstructed perturbation's conductivity changes.

Accepted Manuscript

3. Results

3.1. Resistor phantom

Noise across all channels was 1.87 μV ± 1.12 μV (0.014% ± 0.012%); SNR was 79.3 dB ± 5.15 dB; THD was -60.8 dB ± 1.8 dB ; and mean inter channel variation 0.35 %.

3.2. Scalp Recordings

3.2.1. EEG Noise in the EIT measurements was 1.51 μV ± 0.85 μV and mean SNR value was 61.6 dB ± 4.2 dB (0.09% ± 0.1%). The PSD was extracted for the eyes opened and eyes closed cases, without EIT Figure 2A and with EIT Figure 2B . There was a clear increase in alpha and beta band activity in both cases. There was no significant difference in the EEG for eyes open or closed with or without FDM EIT applied. A t-test across all frequency bins yield a p-value of 0.34 (eyes open) and 0.47 (eyes closed). When comparing isolated frequency bins, statistical difference (P<0.01) was found in 3.5% of bins. However, these results did not repeat across electrodes, nor did they occur in adjacent bins, with the exception of 50 Hz. As such, it is reasonable to attribute these to system noise and EEG variation rather than an effect of the EIT stimulation.

3.2.2. Visual Evoked Potentials The 50 Hz noise increased from 1.03 μV ± 1.06 μV to 1.65 μV ± 2.18 μV when EIT was used. This was attributed to noise pickup from the additional cabling present in the system and prompted the use of the 50 Hz notch filter, commonly used in other EEG assessments, but the signal latency was unaffected. P100 and N145 are clearly visible Figure 2C, latency differences were < 0.2 ms in P100 and N145 in global average all three channels. Considering bins of 100 samples, there was no significant difference in latency (P=0.464) or the peak voltage (P=0.611) of P100 with and without EIT present.

3.2.3. Cardiosynchronous A clear, repeatable ECG gated component was present in the EIT δZ signal Figure 2D, with peak amplitudes ranging from approximately 0.2 to 5 μV or 0.005 to 0.07 %. The impedance increases to a peak at approximately 200 ms after the R wave, with a sharp decrease at the start of T wave, corresponding to a relaxation of the heart. Typically, the Pulse Arrival Time (PAT) is reported, but the inflexion point is unclear in these results, however the peak time is consistent to that observed in other studies in the chest (Proença et al., 2016; Braun et al., 2018).

3.3. Tank Experiments

3.3.1. Static Perturbations The mean noise value across all EIT measurements was 0.70 μV ± 0.21 μV (0.36% ± 0.02%). The mean SNR was 69.95 dB ± 3.5 dB. The reconstructions using an FDM-EIT protocol (12 injections), Figure 3, are qualitatively similar to those in previous studies using a larger TDM-EIT protocol (32 injections),

Accepted Manuscript

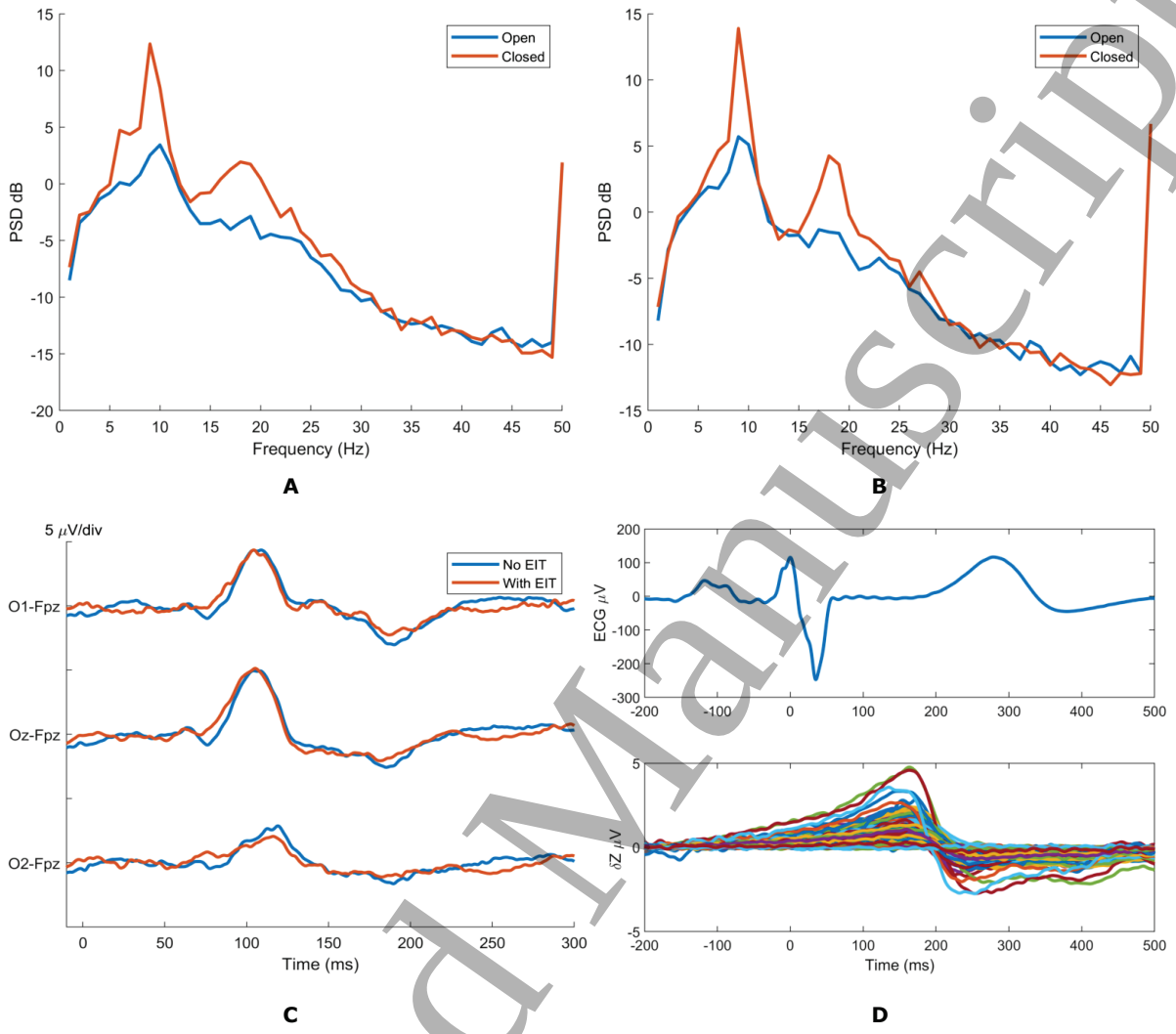

Figure 2. Simultaneous EEG and EIT on human scalp. Comparison of EEG mean PSD across all trials with eyes open and closed at electrode Oz with (A) no EIT system connected (B) EIT system connected and injecting. Increase in alpha activity visible, and no significant difference in PSD detected in any electrodes P=0.34 (eyes open) and P=0.47 (eyes closed). (C) VEP study, P100 latency unchanged (P=0.464) with EIT present (D) ECG gated cardiosynchronous δZ signals (0.005 to 0.07 %) present in scalp recordings.

despite the lower number of injections used. However, there were increased positive artefacts and perturbation distortion (Avery, Aristovich, Low and Holder, 2017; Dowrick and Holder, 2018). This is reflected in the image quantification metrics, where the mean localisation error, 2.6% was lower than shape or noise error, 8.7% and 12.2% respectively. The anterior position had the lowest of all three error metrics with 18% total error, compared to 31.6% and 20.0% in the posterior and lateral positions. EEG inverse reconstructions were successful during EIT measurements, but with considerably larger shape distortion as the perturbation was drawn towards the frontal area. This contributed to a significantly larger image error scores of 90.2% compared to 23.5% for

Accepted Manuscript

EIT.

3.3.2. EEG Comparison No significant difference was present between the EEG data recorded with or without EIT, in either the raw voltage signal, Figure 5a (p-value >0.05), or the PSD magnitude (p-value > 0.05) Figure 5b. The magnitude-squared coherence was γ^2 0.967 ± 0.046, suggesting a highly linear correlation across the whole spectra. The correction coefficient across all 32 channels was 0.93 ± 0.061.

3.3.3. Dynamic Experiments A single perturbation was successfully reconstructed in every frame during the dynamic experiments, Figure 6 and Supplementary Materials. The trajectory follows the programmed sequence showing the perturbation entering the tank, then moving between four perturbation locations. As with the static perturbations, the shape error was uneven across the head, increasing in the posterior and lateral locations.

4. Discussion

The Noise and SNR values measured in the resistor phantom were comparable to those previously reported for the UCL ScouseTom system (Avery, Dowrick, Faulkner, Goren and Holder, 2017), and the SNR during scalp electrodes was superior to those recorded in the ScouseTom in stroke patients and healthy subjects (Goren et al., 2018). This can be attributed to the reduction of wiring, and the implementation of a fully battery powered floating parallel current source. The values are also in line with desired noise values (<0.1 %) for clinical recording of epileptic activity (Fabrizi et al., 2006). The level of inter channel variation can be attributed to the use of 1 % tolerance resistors and 5 % tolerance capacitors in the fabricated current source. Therefore, this can be improved using components with a better tolerance, or through combining multiple components in parallel.

Data collected using the EEG dipole, scalp EEG and VEP recordings demonstrated that unaffected EEG can be collected alongside EIT data. The EEG signal could be recovered and displayed in real time through the use of in-built filters in the actiCHamp software, or by offline filtering in MATLAB. As the signal was unaffected on both measurement and stimulation electrodes, the total number of parallel injections could be increased to allow for more data to be collected. As a maximum, every electrode could be used for injection, giving 16 injection pairs for the same 32 electrode montage used on stroke patients (Goren et al., 2018).

In the tank, despite the reduced injection protocol, it was still possible to reconstruct a physiologically representative perturbation throughout the brain, tracking the trajectory of the centre of mass with a frame rate of 20 Hz, Figure 6. Whilst no such perturbation was present in healthy subjects, the cardiosynchronous signal Figure 2d, demonstrated the method is capable of detecting impedance changes of the order of 0.01 % with a time course of approximately 200 ms when combined with coherent averaging.

Accepted Manuscript

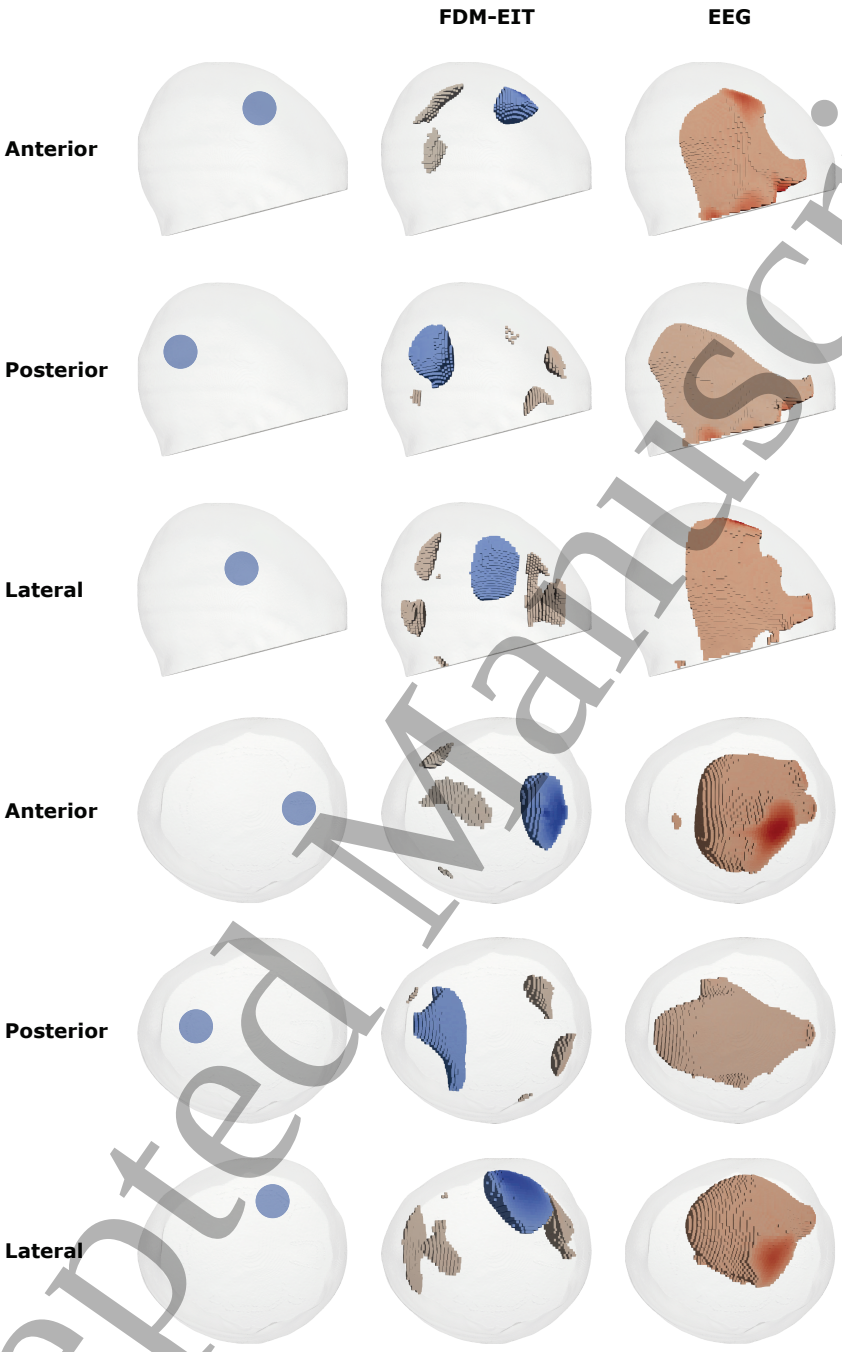

Figure 3. Comparison of FDM EIT and EEG image reconstructions of colocated perturbation and dipole in neonatal head tank in three positions: Anterior, Posterior and Lateral. FDM-EIT reconstructions with 12 simultaneous injections, EEG inverse using the peak value in Figure 5a. FWHM of positive and negative changes shown

Accepted Manuscript

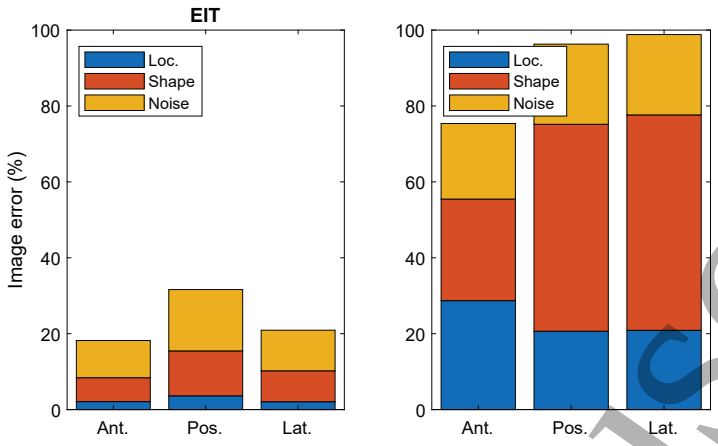

Figure 4. Comparison of Image quantification metrics for FDM-EIT and EEG inverse reconstructions

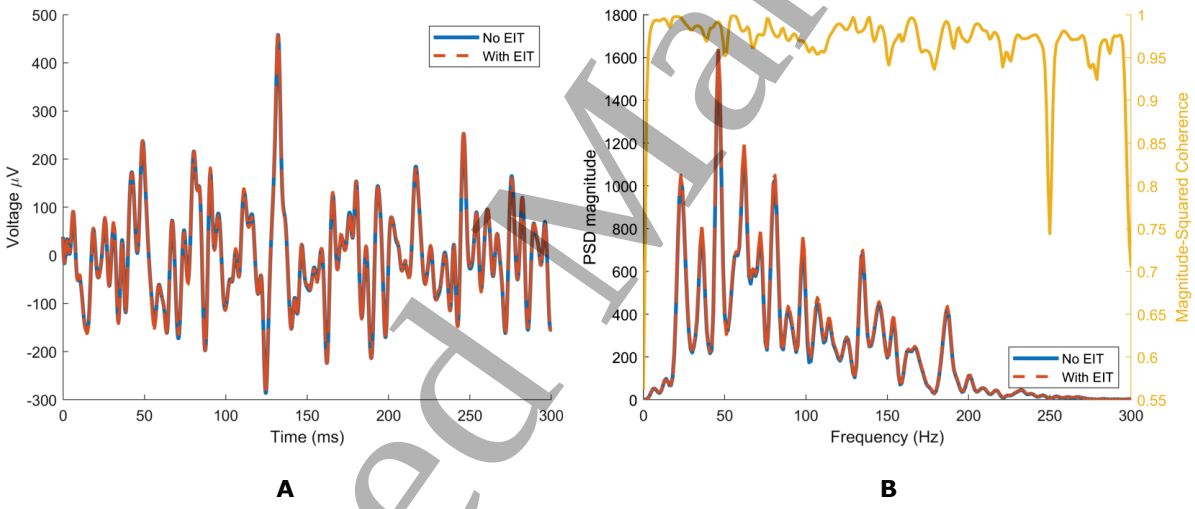

Figure 5. Recovering the EEG dipole signal in the head tank during EIT current injection, comparing (A) the EEG voltages recorded r= 0.93 ± 0.061 (B) the PSD of EEG signal, and spectral coherence γ^2 0.967 ± 0.046

This suggests that it is suitable for long term monitoring applications, using either the Inter Ictal Spike (IIS) triggered signals Vongerichten et al. (2016) or seizure induced cell swelling signals, expected to be of the order 0.1 % on the scalp Fabrizi et al. (2006). Whilst the EEG inverse could be improved using specialsied inverse source methods Vanrumste et al. (2008); Michel et al. (2004), the direct comparison in Figure 3 shows the potential for EIT to provide additional diagnostic data, without altering clinical workflows.

Image quantification metrics for static tank images were found to be consistent with previously published values, with a localisation error of 2.6 % compared to 2.6 % (Avery, Aristovich, Low and Holder, 2017) and 2.8 % (Dowrick and Holder, 2018) in previous

Accepted Manuscript

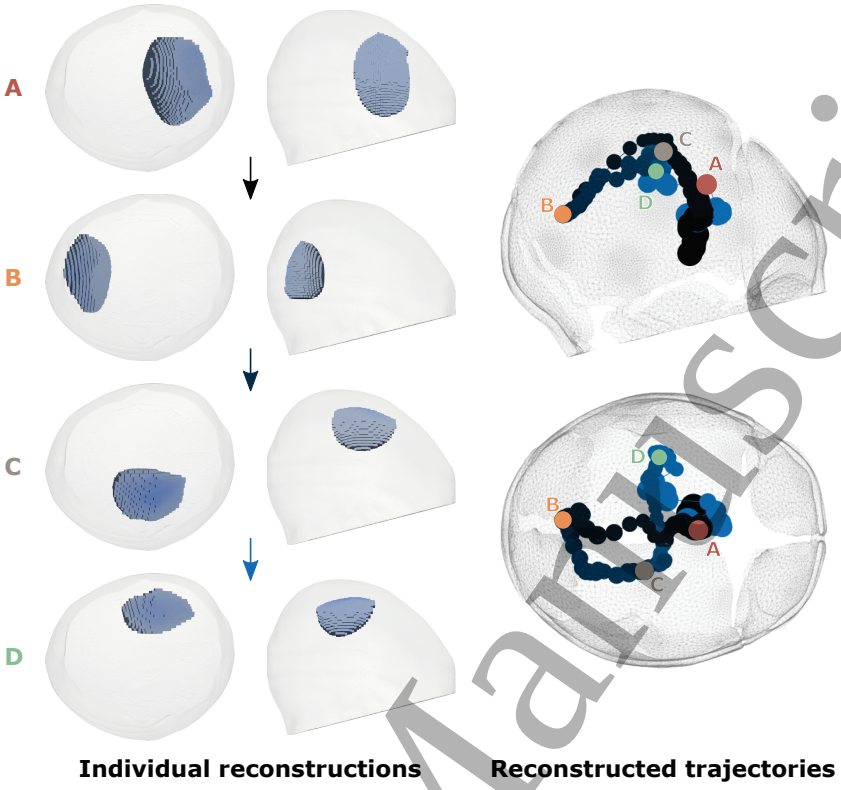

Figure 6. Trajectory of centre of mass (COM) during dynamic experiments. Left: FWHM reconstructions of four example positions Right: Trajectory of the calculated COM at each 50 ms frame. Perturbation enters the tank before moving between anterior (A) posterior (B) caudal (C) and lateral (D) positions. Time is indicted by the colour of the marker, black at t=0 and blue at t=10.5 s. The size of the image marker is representative of the size of the reconstructed volume.

studies in the same phantom. Overall however, there was a reduction in image quality compared to sequential EIT with larger numbers of injections, which is consistent with expectations and is one of the necessary trade-offs when using FDM-EIT due to the limited number of injections possible. Whilst the localisation error was consistent across the head, including more locations in this study has made clear the increased spatial dependence of the reconstructed image quality. This is evident in the reconstructed shape error, which doubled in the posterior and lateral locations, both areas which were not prioritised by the current injection selection algorithm. This uneven coverage resulted in an uneven sensitivity, and thus greater errors in these locations. This effect is more pronounced when using only 12 injection pairs compared to c. 32 as in previous studies with this phantom (Avery, Aristovich, Low and Holder, 2017).

4.1. Technical Limitations and Recommendations for Use

Careful choice of injection frequencies is recommended for parallel EIT, in order to maximise the signal amplitude. As a minimum, the spacing between frequencies should

Accepted Manuscript

be greater than twice the filter bandwidth used during the signal processing phase, to avoid contamination between signals. Further, it is desirable to keep all frequencies within one octave of the fundamental, so that harmonics do not affect higher frequencies. In practice, this can be difficult to achieve, as it must be balanced against the frequency range in which the signal is present, and the recording capability of the EEG amplifier (20 kHz in this case). If a region can be targeted *a priori* then the EIT protocol can be further optimised to maximise the sensitivity within the ROI.

The approach described in this work is well suited to impedance changes with a predominately resistive component (cell swelling, blood flow, pulsatility) which occur over a wide frequency range, as the spectral range can accommodate sufficient current injections with the required bandwidth separation. It is less well suited to fast changing signals with limited signal range. For example, fast neural epilepsy signals have bandwidth requirements >1 kHz, requiring 2 kHz spacing between frequencies, allowing only two injections in the usable frequency range, up to ≈3.5 kHz (Hannan, Faulkner, Aristovich, Avery and Holder, 2018; Faulkner et al., 2018). For comparison, the slow impedance change has a usable frequency range up to ˜10 kHz and bandwidths as low as 1 Hz can be used (Hannan, Faulkner, Aristovich, Avery and Holder, 2018).

In this work, the same EEG system was used to collect both the EEG and EIT data. This limits the usable recording systems to high specification research systems (BioSemi, actiCHamp, g.tec). At present, only the g.tec system has a CE marking for clinical use, but this is not widely used clinically. Most clinical settings will use an EEG system with a lower sampling rate (e.g. Micromed or Natus Quantum LTM Amplifier). As such, it would be necessary to use a separate recording system to collect EIT data. Depending on the design of the clinical system being used, it may be necessary to implement custom hardware filters or DC blocking, to avoid saturation of the clinical amplifiers inputs. For example, the Micromed system has a dynamic range of only several mV (compared to ≈0.5 V for research systems), and the input amplifiers can easily become saturated by small DC offsets present on EIT injection channels, obscuring any EEG signal. Many EEG amplifiers implement oversampling to reduce noise and increase resolution, in which case the lowest EIT injection frequency used would be constrained by the ADC sampling frequency, not the EEG bandwidth.

The current system has battery life in excess of five hours, making it feasible for use in long term telemetry recordings, such as those used to capture epileptic seizures. Care should be taken to reduce cable lengths, and to use shielded cables where possible, to minimise interference from mains power sources.

Acknowledgment

This article is independent research funded by the National Institute for Health Research (NIHR) Imperial Biomedical Research Centre (BRC). The views expressed in this publication are those of the author(s) and not necessarily those of the NHS, the National Institute for Health Research or the Department of Health. This work was supported

Accepted Manuscript

by EPSRC grant EP/M506448/1, DARPA grant N66001-16-2-4066 and The Wellcome Trust.

Appendix A. Software

The signal processing software used are available at `https://github.com/EIT-team/Load_data` or archived in DOI:10.5281/zenodo.1479817

The models and code used to create the head phantoms and injection protocol is found at `https://github.com/EIT-team/Tanks`, and `https://github.com/EIT-team/Injection-Protocol` or archived at DOI:10.5281/zenodo.1489106.

The MeArm control software and tank frame are available at `https://github.com/EIT-team/MotorStuff` and archived at DOI:10.5281/zenodo.1489788.

The EEG source hardware and software are in `https://github.com/EIT-team/EEGSource` archived DOI:10.5281/zenodo.1489804

The EIT forward and inverse solvers were `https://github.com/EIT-team/PEITS` and `https://github.com/EIT-team/Reconstruction` archived at DOI: 10.5281/zenodo.1641128 and DOI: 10.5281/zenodo.1643416

All resources are released under a GNU General Public License v3.0.

Appendix B. Hardware

The EIT system used a custom 6-channel current source PCB (B1) and the actiCHamp EEG system (Brain Products GmbH) for simultaneous voltage recording at 100 kHz. An Arduino Pro Micro sets the frequency of each current source individually, and the amplitude is controlled by a jumper setting on the current source output stage. Each individual current source (B2) used an AD9833 DDS IC for sine wave generation. A 2nd order image filter (OP1) on the AD9833 output line reduces the high frequency components present in the sharp edges of the DDS signal, and the DC component of the signal is removed (OP2). The voltage waveform is converted to a double ended signal (OP2 and OP3) and a differential Howland current pump (OP5 and OP6) is used to perform V-I conversion. The differential current pump was used in place of the 'standard' HCP, to prevent interference between different injection currents. A jumper on the HCP output stage allows for selection of the gain resistor, to set the output current to 120 uA, 60 uA, 30 uA or 12 uA.

A Lithium Polymer battery provides +3 V, with an on-board USB charging circuit, and a LTC1044 generates the negative voltage rail. OPA2188 dual package op-amps were used. Resistors in the HCP stage were 0.1% tolerance; all other resistors were 1%, and capacitors 5%. Component values are given in B1. The layout of each current source within the PCB was identical, to reduce any inter channel variation.

Schematic and layout files (Altium), PCB Gerber files and a BOM are available on the project GitHub page `https://github.com/EIT-team/Parallel_CS_Altium`, or archived at DOI:10.5281/zenodo.1489110.

Accepted Manuscript

Component	Value
R1	715 Ω
R2	13k Ω
R3, R4, R5, R6, R7	10k Ω
R8, R9, R11, R12, R13, R14, R16, R17	100k Ω
R10, R15	5k/10k/20k/50k Ω
C1	220pF
C2	2.2nF
C3	1uF

Table B1. List of Component Values

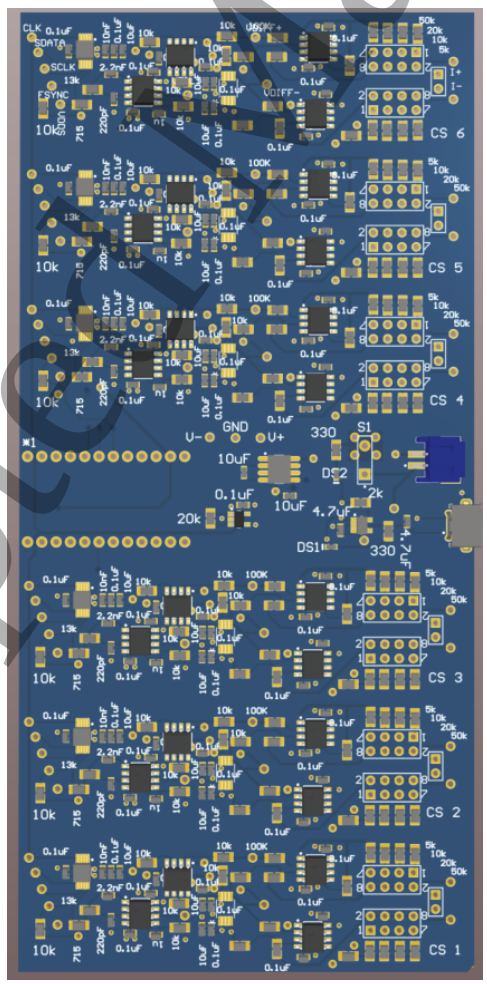

Figure B1. 6 Channel Current Source PCB

Accepted Manuscript

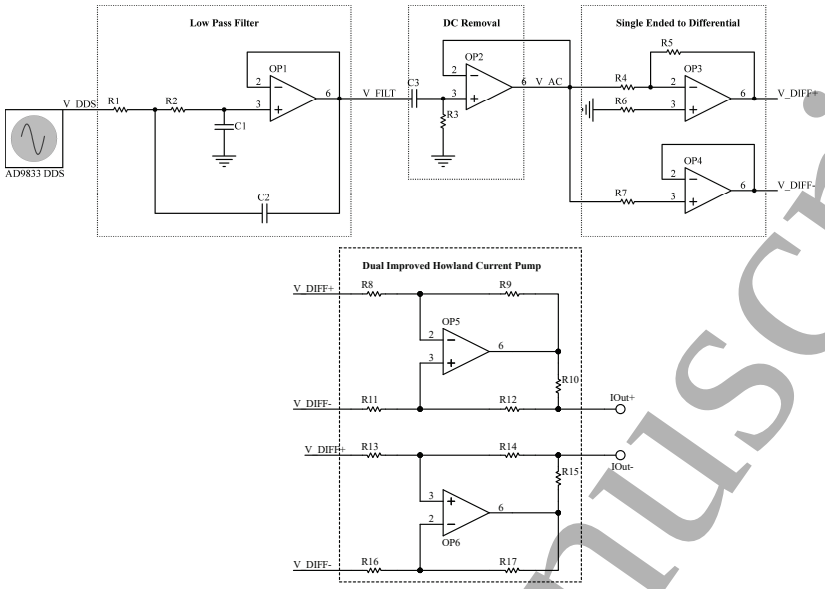

Figure B2. Single Current Source Implementation

Appendix B.1. Output impedance

Output impedance of each source was measured for all six current sources, with values in excess of 100 kΩ measured for all frequencies of interest. While this is sufficient for these investigations, it is lower than some other reported systems. The necessary use of a differential HCP in the output stage is primarily responsible, as even with 0.1% resistor tolerances, the effects of mismatches are more pronounced than for the single ended HCP which is more commonly employed in EIT systems.

References

Adler A, Proença M, Braun F, Brunner J X and Solà J 2017 p. 2010.

Andrew R and Macvicar B 1994 *Neuroscience* **62**(2), 371–383.

Aristovich K, Donegá M, Blochet C, Avery J, Hannan S, Chew D J and Holder D 2018 *Journal of Neural Engineering* **15**(5), 056025.

Aristovich K Y, dos Santos G S, Packham B C and Holder D S 2014 *Physiological Measurement* **35**(6), 1095–1109.

Aristovich K Y, Packham B C, Koo H, dos Santos G S, McEvoy A and Holder D S 2016 *NeuroImage* **124**, 204–213.

Avery J, Aristovich K, Low B and Holder D 2017 *Physiological Measurement* **38**(6), 1116–1131.

Avery J, Dowrick T, Faulkner M, Goren N and Holder D 2017 *Sensors* **17**(2), 280.

Benbadis S R, Neill E O, Tatum W O and Heriaud L 2004 *Epilepsia* **45**(9), 1150–1153.

Binder D K and Haut S R 2013 *Epilepsy & behavior* **26**(3), 247–52.

Accepted Manuscript

Boone K, Lewis A and Holder D 1994 *Physiological measurement* **189**.

Braun F, Proença M, Adler A, Riedel T, Thiran J P and Solà J 2018 *PLOS ONE* **13**(1), e0191870.

Broberg M, Pope K J, Lewis T, Olsson T, Nilsson M and Willoughby J O 2008 *Epilepsy research* **80**(2-3), 132–41.

Burle B, Spieser L, Roger C, Casini L, Hasbroucq T and Vidal F 2015 *International Journal of Psychophysiology* **97**(3), 210–220.

Dowrick T and Holder D 2018 *Physiological Measurement* **39**(3), 034005.

Ebersole J S 1997 *Epilepsia* **38**(s4), S1–S5.

Fabrizi L, Sparkes M, Horesh L, Abascal J F P J, McEwan A, Bayford R H, Elwes R, Binnie C D and Holder D S 2006 *Physiological Measurement* **27**(5), S163–S174.

Fabrizi L, Yerworth R, McEwan A, Gilad O, Bayford R and Holder D S 2010 *Physiological Measurement* **31**(8), S57–S72.

Faulkner M, Hannan S, Aristovich K, Avery J and Holder D 2018 *Physiological Measurement* **39**(3), 034007.

Faulkner M, Jehl M, Aristovich K, Avery J, Witkowska-Wrobel A and Holder D 2017 *Physiol Meas* **38**, 1158–1175.

Gilad O and Holder D S 2009 *NeuroImage* **47**(2), 514–522.

Goren N, Avery J, Dowrick T, Mackle E, Witkowska-Wrobel A, Werring D and Holder D 2018 *Scientific Data* **5**, 180112.

Halter R J, Hartov A and Paulsen K D 2008 *30th Annual International IEEE EMBS Conference* pp. 1192–1195.

Hannan S, Faulkner M, Aristovich K, Avery J and Holder D 2018 *Physiological Measurement* **39**(8), 085003.

Hannan S, Faulkner M, Aristovich K, Avery J, Walker M and Holder D 2018 *NeuroImage: Clinical* **20**, 674–684.

Harreveld A V and Schadé J 1962 *Experimental Neurology* **5**(5), 383–400.

Holder D 2004 *in* 'Series in Medical Physics and Biomedical Engineering' Taylor & Francis.

Jehl M, Dedner A, Betcke T, Aristovich K, Klofkorn R and Holder D 2015 *IEEE Transactions on Biomedical Engineering* **62**(1), 126–137.

Kramer M A and Cash S S 2012 *Neuroscientist* **18**(4), 360–372.

Malone E, Jehl M, Arridge S, Betcke T and Holder D 2014 *Physiological Measurement* **35**(6), 1051–1066.

Meckl P H, Arestides P B and Woods M C 1998 *Proceedings of the American Control Conference* **5**(June), 2627–2631.

Meinardi H, Scott R A, Reis R and on J W A S S O B O T I C 2008 *Epilepsia* **42**(1), 136–149.

Accepted Manuscript

Michel C M, Murray M M, Lantz G, Gonzalez S, Spinelli L and Grave De Peralta R 2004 *Clinical Neurophysiology* **115**(10), 2195–2222.

Murray D M, Boylan G B, Ali I, Ryan C A, Murphy B P and Connolly S 2008 *Archives of Disease in Childhood - Fetal and Neonatal Edition* **93**(3), F187–F191.

NeurophysiologySociety A C 2006 *Journal of Clinical Neurophysiology* **23**. Accessed on Tue, October 09, 2018.

Oostenveld R and Praamstra P 2001 *Clinical Neurophysiology* **112**(4), 713–719.

Proença M, Braun F, Solà J, Adler A, Lemay M, Thiran J P and Rimoldi S F 2016 *Physiological Measurement* **37**(6), 713–726.

Rosell J, Colominas J, Riu P, Pallas-Areny R and Webster J 1988 *IEEE Transactions on Biomedical Engineering* **35**(8), 649–651.

Somersalo E, Cheney M and Isaacson D 1992 *SIAM Journal on Applied Mathematics* **52**(4), 1023–1040.

Tidswell T, Gibson A, Bayford R H and Holder D S 2001 *NeuroImage* **13**(2), 283–294.

Vallaghé S, Papadopoulo T and Clerc M 2008 *Physics in Medicine and Biology* **54**(1), 135–147.

Vanrumste B, Grech R, Zervakis M, Camilleri K P, Cassar T, Muscat J, Sakkalis V, Xanthopoulos P and Fabri S G 2008 *Journal of NeuroEngineering and Rehabilitation* **5**(1), 25.

von Ellenrieder N, Beltrachini L and Muravchik C H 2012 *Clinical Neurophysiology* **123**(9), 1745–1754.

Vongerichten A N, dos Santos G S, Aristovich K, Avery J, McEvoy A, Walker M and Holder D S 2016 *NeuroImage* **124**, 813–823.

Walsh P 2005 *Journal of Neurology Neurosurgery & Psychiatry* **76**(suppl_2), ii16–ii22.

Wang L, Sun Y, Xu X, Dong X and Gao F 2017 *NeuroReport* **28**(11), 689–693.

Weiner S, Painter M, Geva D, Guthrie R and Scher M 1991 *Pediatr Neurol* **7**, 363–8.

Wellmer J, Von Der Groeben F, Klarmann U, Weber C, Elger C E, Urbach H, Clusmann H and Von Lehe M 2012 *Epilepsia* **53**(8), 1322–1332.

Witkowska-Wrobel A, Aristovich K, Faulkner M, Avery J and Holder D 2018 *NeuroImage* **173**, 311–321.

Accepted Manuscript